Tropical Cyclone Rainfall

ROBERT ROGERS[1], FRANK MARKS[1] AND TIMOTHY MARCHOK[2]

[1]NOAA/AOML Hurricane Research Division, Miami, FL, USA
[2]NOAA Geophysical Fluid Dynamics Laboratory, Princeton University Forrestal Campus, Princeton, NJ, USA

A brief survey of the relevant research of tropical cyclone (TC) rainfall is presented here. The importance of TC rainfall in global and regional rainfall budgets is discussed, as is its mean characteristics as derived from airborne and satellite observational studies. Discussion is also presented on the physical processes that can modulate TC rainfall distributions, including topography, storm motion, vertical shear, and extratropical transition. Some tools that have been developed to predict and evaluate forecasts of TC rainfall are discussed. Finally, a summary and outlook for the future is presented, including a discussion of opportunities for improving TC rainfall forecasts and conducting research into the role of TC rainfall in intensity and structure changes in TCs.

INTRODUCTION

Q3 One of the• most significant impacts of tropical cyclones
Q4 (TCs) is the copious amount of rainfall• they often produce. This heavy rainfall often can lead to loss of life and property. In fact, before Hurricane Katrina in 2005, drowning from inland flooding in landfalling TCs was the leading cause of death from storms affecting the United States in the past 30 years (Rappaport, 2000). The importance of correctly forecasting rainfall amounts and the potential for flash floods from TCs is, thus, critical to saving lives. In addition to the threat to human life, fresh water flooding from TCs has major economic impacts. In 2001, for example, flooding in the Houston area from Tropical Storm Allison (Figure 1) generated more than $6 billion in total damage, of which $2.5 billion was insured. TC rainfall can also have significant impacts on regional water budgets. For example, in a study of heavy rainfall events with recurrence intervals of 5 years and greater in the eastern half of the Carolinas from 1950 to 2004, Konrad and Perry (2009) found that 90% of these events were related to the passage of TCs. An analysis by Villarini and Smith (2009) of stream and river gaging stations in the eastern United States with a record of at least 75 years showed that for numerous locations in Florida and along the East Coast from South Carolina through southern New Jersey, at least half of the 10 largest flood peaks were caused by TCs.

Despite these detrimental impacts, TC rainfall can also bring benefits to many parts of the globe. For example, it can contribute as much as 15–17% of the total annual rainfall over a broad latitude band around the globe (Figure 2). Regionally, the contributions can be even more significant, with TCs having recently been attributed as contributing as much as 15% of total hurricane-season rainfall in the Carolinas (Knight and Davis, 2007). Figure 3 shows the contributions of TC rainfall to the total summer rainfall in central and southern Florida for 2003 and 2004. In 2003, only one TC impacted the region (Figure 3a), while in 2004 four TCs impacted the area (Figure 3b). In 2003, TCs accounted for less than 10% of the total summertime rainfall over the peninsula (Figure 3c), while in 2004 TCs accounted for more than 50% of the total summer rain (Figure 3d). Other regions of the globe also experience significant contributions from TC rainfall (Figure 4), for example, the northeast Pacific from western Mexico extending into the Pacific west of Baja, northwest Australia from Northern Territory east to Gulf of Carpentaria, the southwest Indian Ocean from the African east coast over Madagascar toward La Reunion, the northwest Indian Ocean south of the Red Sea region, the northwest Pacific Ocean from China eastward to about 150E, the Subtropical

Figure 1 Flooding in Houston, TX, in aftermath of Tropical Storm Alison (2001). (Credit: Dave Einsel, Houston Chronicle)

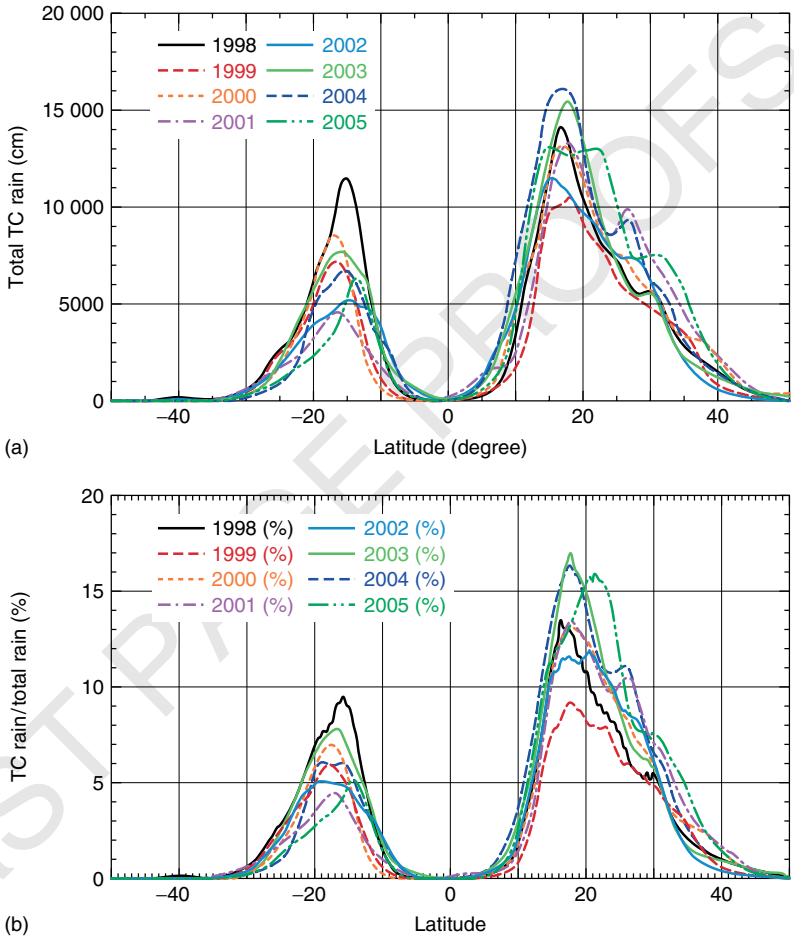

Figure 2 (a) Total rainfall (centimeter) in each 1° latitude belt as a function of latitude attributable to tropical cyclones in designated years, as defined by runs of the rainfall-CLIPER (Tuleya *et al.*, 2007) model along observed tracks and (b) percentage of total rainfall contributed from tropical cyclones

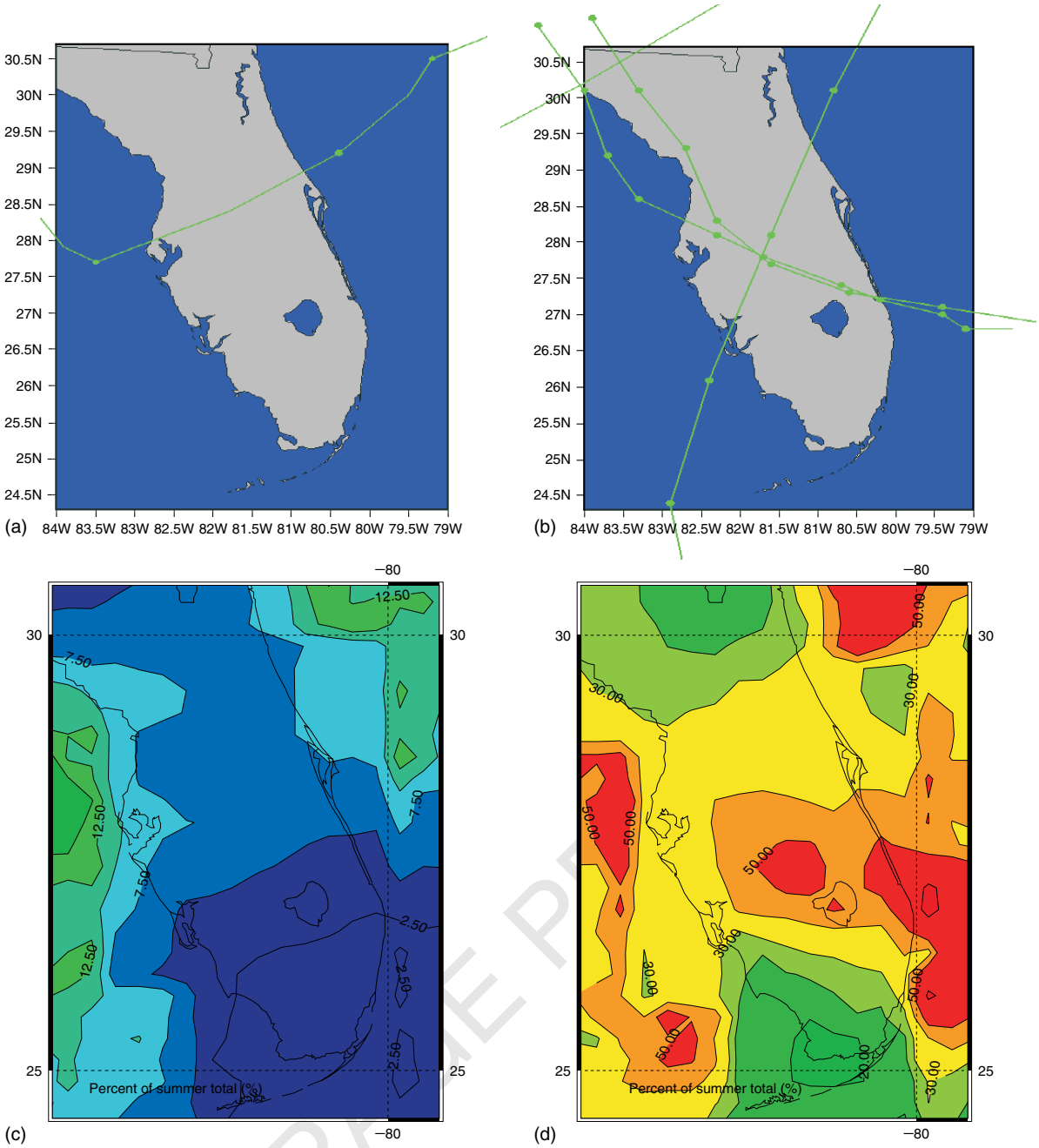

Figure 3 (a) Tracks of tropical cyclones making landfall in Florida for 2003; (b) as in (a), but for 2004; (c) contribution of tropical cyclone rainfall to total summertime rainfall in central and southern Florida for 2003; and (d) as in (c), but for 2004

Atlantic from Gulf of Mexico eastward toward W. Africa, the Bay of Bengal, and the south Pacific northeast of Australia. In these regions, TC rainfall contributes up to 25% of total annual rainfall, and in the case of Mexico TCs contribute >50% of the rainfall. This very high percentage is because the area is otherwise a desert, and without TCs this area would be much drier. Such differences in TC frequency and its associated rainfall contributions can have significant implications for water and agricultural management and planning. With all of these impacts, the need to better characterize, understand, and predict TC rainfall is thus of paramount importance.

The TC circulation dynamically constrains convective development and rainfall to storm-relative locations (e.g. eyewall, rainband, and stratiform regions, which are discussed later) that may persist for time periods from

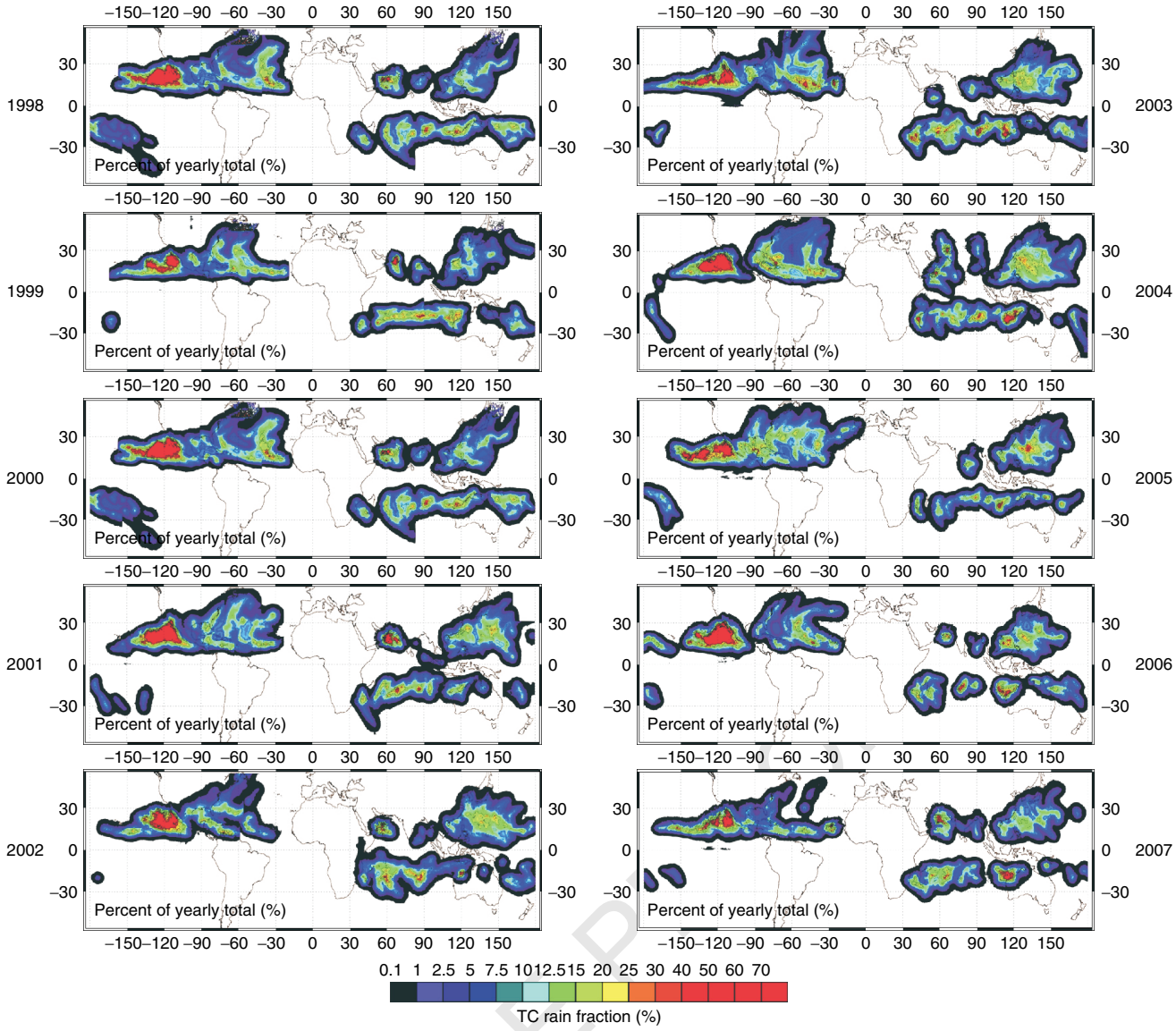

Figure 4 Proportion of annual rainfall contributed by tropical cyclones (as estimated using observed TC tracks and Rainfall-CLIPER model (Tuleya *et al.,* 2007)) compared with total annual rainfall measured by TRMM 3B-43 monthly rainfall product for years 1998–2007

hours to days. These features, thus, have some degree of predictability that, when combined with accurate predictions of storm track and intensity and interactions with topography and other environmental features, can allow for improved skill in TC rainfall forecasting. These dynamical constraints also provide an ideal laboratory for conducting research that targets these specific rainfall-producing regions. Such research, largely from airborne and ground-based radar, rain gauge networks, and satellites, has provided a detailed picture of the processes that produce and modulate the spatial and temporal distribution of TC rainfall. The purpose of this article is to describe the findings of this research, including the characteristics of TC rainfall, the processes that modulate it, and the techniques that predict it.

CHARACTERISTICS OF TC RAINFALL

Mature TCs (called *hurricanes* in the Atlantic and East Pacific basins, *typhoons* in the western Pacific basin, and *cyclones* in the Indian basin) are dominated by two primary precipitation processes common in convective rain systems across the globe: convective, in which hydrometeors form at low levels and are carried upward by strong updrafts

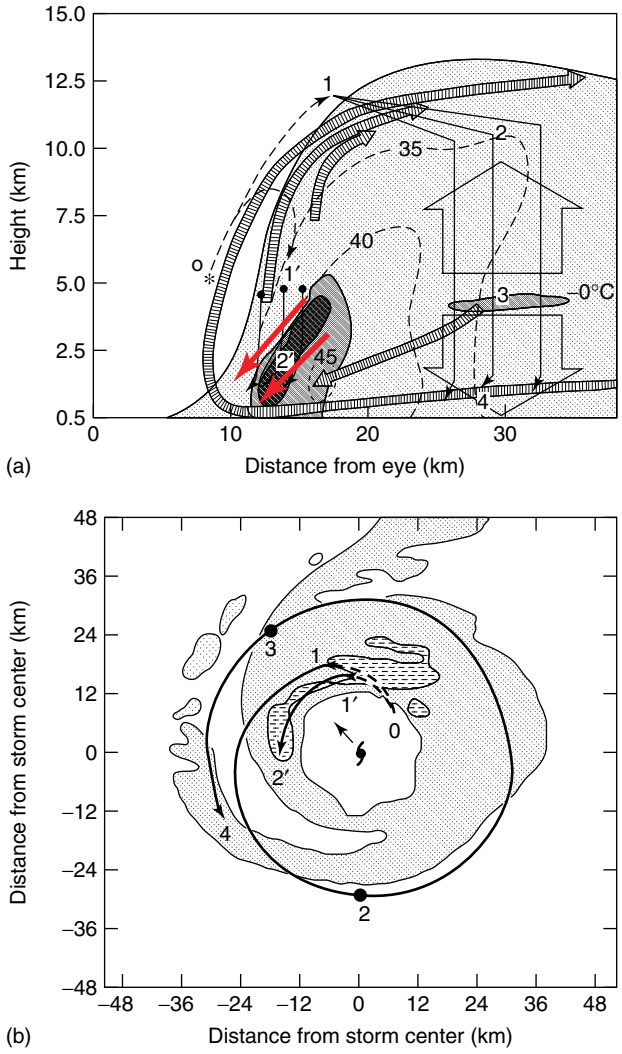

Figure 5 (a) Schematic of the radius–height circulation of the inner core of Hurricane Alicia (1983). Shading depicts the reflectivity field, with contours of 5, 30, and 35 dBZ. The primary circulation (azimuthal, meter per second) is depicted by dashed lines and the secondary circulation by the wide hatched streamlines. The convective downdrafts are denoted by the thick red arrows, while the mesoscale updrafts and downdrafts are shown by the broad arrows. The level of the 0 °C isotherm is labeled. (b) A schematic plan view of the low-level reflectivity field in Hurricane Alicia superimposed with the middle of three hydrometeor trajectories in (a). The reflectivity contours are 20 and 35 dBZ. The hydrometeor trajectories are denoted by dashed and solid line labeled 0-1-2-3-4 and 0-1′-2′. (From Marks and Houze (1987). Reproduced by permission of American Meteorological Society)

until they grow to sufficient size to fall out, and stratiform, in which vertical air motions are weak and precipitation particles drift down from the upper reaches of the cloud toward the earth's surface as they grow. Both of these processes are evident in the schematic in Figure 5 as illustrated by particle trajectories derived using airborne Doppler radar (Marks and Houze, 1987). Convective-scale updrafts predominate in the inner core as a key part of the ascending branch of the cyclone's secondary circulation, termed the *eyewall*. The strong updrafts in this region inject hydrometeors into the upper troposphere, where some of them fall in convective downdrafts (bold red arrows around 12–15 km radius) just outside the updrafts. Other hydrometeors are transported radially outward to the stratiform region, where they fall slowly through regions of weak mesoscale ascent (broad arrow at 30 km radius) and continue to grow through deposition and aggregation processes before falling through a mesoscale downdraft originating just below the melting level. As the hydrometeors complete the radial-vertical, in-up-out circuit described here, they can also be advected several times around the cyclone in the strong tangential flow (Figure 5b), a process termed the *mix master* in Marks and Houze (1987). Generally, the heaviest precipitation is associated with the convective-scale structures in the inner core, whereas lighter precipitation predominates in the stratiform regions radially outward. It should be stressed, though, that the areal coverage of the heavier convective precipitation in the eyewall is much smaller than that of the stratiform precipitation, so that total rainfall amounts can be comparable between the stratiform and the eyewall regions of the storm.

The precipitation structure in mature TCs is composed of several distinct structural features (Figure 6a, from Dodge *et al.*, 1999). The primary feature associated with these storms is the eyewall, which is a ring of heavy precipitation and high winds wrapped around the center of circulation (and occasionally accompanied by an outer eyewall as shown in Figure 6a). In intense TCs, the eyewall is typically convective, with radar reflectivities as high as 50 dBZ. This reflectivity value is equivalent to rainfall rates of 74 mm h^{-1} (Marks, 2003) using tropical Z–R relationships such as that from Jorgensen and Willis (1982). The spiral rainbands are outside of the eyewall, which contain a mixture of convective and stratiform rainfall. The convective cores within rainbands are typically of a smaller magnitude than that seen in the eyewall (40 dBZ, equivalent to 13 mm h^{-1}). Precipitating areas not within the eyewall or rainbands are primarily classified as stratiform precipitation. These areas, which are usually more horizontally homogeneous and cover a broader area, contain precipitation with maximum reflectivities of 30 dBZ (2.4 mm h^{-1}).

A vertical cross section of the axisymmetric structure of these precipitation features is shown in Figure 6(b). The eyewall region is seen as a narrow band of high reflectivity that extends over a deep layer, up to 15 km in this case. This region is a part of the upward branch of the cyclone's secondary circulation (Marks and Houze, 1987). An outer eyewall seen in the plan view (Figure 6a) is also evident in

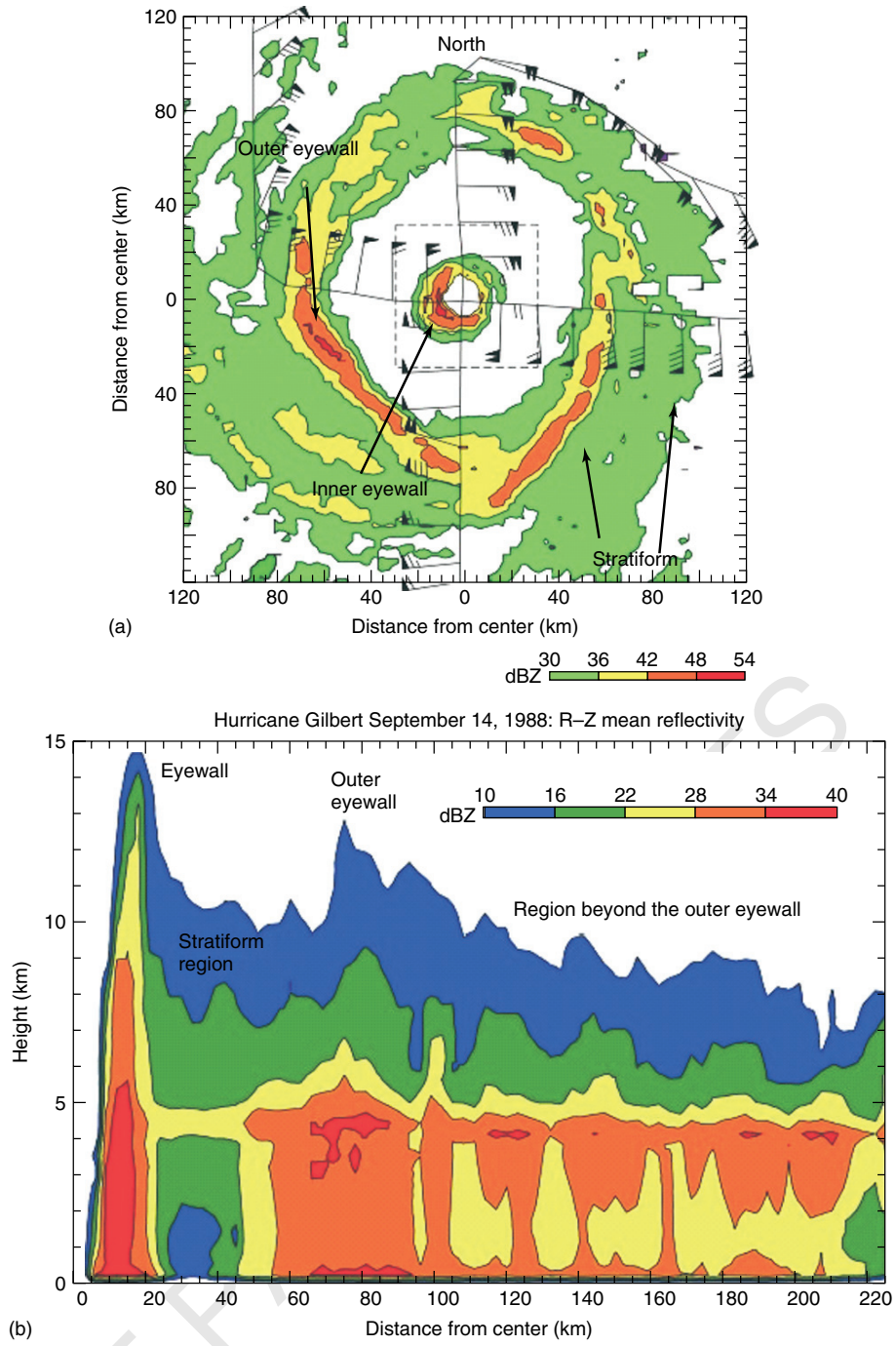

Figure 6 (a) Lower fuselage radar image for Hurricane Gilbert from 10 : 08 to 10 : 15 universal time coordinated (UTC) September 14, 1988. Line with wind barbs is flight track from 08 : 58 to 10 : 16 UTC. Barbs• plotted every 2 min; pennant = 25 m s^{-1}, barb = 5 m s^{-1}. (b) Radius–height cross section of tail radar reflectivity (dBZ) averaged for all four radial legs shown in (a) for region within 225 km of center of Hurricane Gilbert on September 14, 1988. (Adapted from Dodge *et al.* (1999). Reproduced by permission of American Meteorological Society)

this cross section, though its reflectivity values are not as high and it does not extend as deep as the main eyewall. The vast majority of the cross section is dominated by stratiform precipitation. The precipitation is lighter than that in the eyewall at all levels, and it does not extend as deep as either the main or the secondary eyewall. Note that there is no evidence of rainband structures in this axisymmetric cross section, which is partially due to sampling issues with

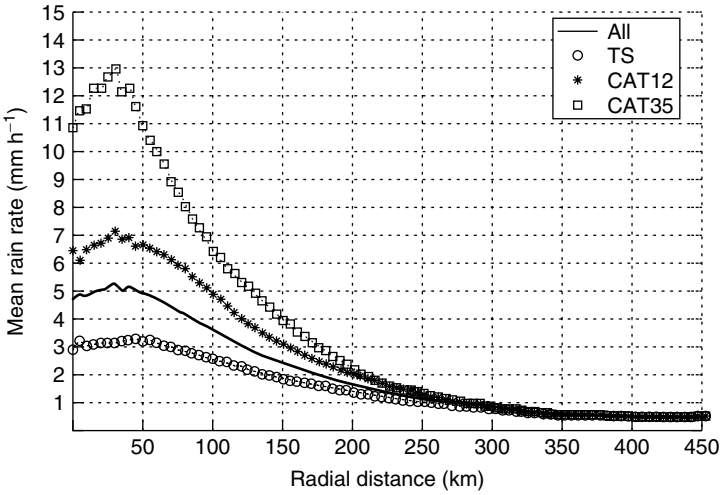

Figure 7 Mean rain rates (millimeter per hour) derived from Tropical Rainfall Measuring Mission (TRMM) Microwave Imager observations of all tropical cyclones from 1998 to 2000 stratified by storm intensity. (From Lonfat *et al.* (2004). Reproduced by permission of American Meteorological Society)

the aircraft and also because, at the radii where rainbands normally reside, they occupy a smaller fraction of a given azimuthal ring than the eyewall and stratiform areas.

Tropical cyclone rainfall varies primarily by radius and intensity. Radial profiles of the axisymmetric mean rainfall rates for storms of different intensities, derived from global satellite measurements of TCs, are shown in Figure 7 (Lonfat *et al.*, 2004). As discussed above, the heaviest rain rates are seen in the eyewall region, as peak rain rates occur at radii less than 50 km. From there the mean rain rate decreases with increasing radius. Mean rain rate increases with increasing storm intensity, with peak rain rates of 13 mm h^{-1} for major hurricanes (Categories 3–5 on the Saffir–Simpson scale; Saffir, 1973; Simpson, 1974), 7 mm h^{-1} for minor hurricanes, and 3 mm h^{-1} for tropical storms. Differences in rain rates among the different storm intensities vanish by 300 km from the center.

Accumulated rainfall from a TC can produce decidedly different rainfall distributions than those from more typical summertime thunderstorms. Figure 8 shows radar-derived 24-h accumulated rainfall totals in Florida for two different regimes: a case of sea-breeze generated summer thunderstorms and the passage of Hurricane Irene (1999). Both cases have peak rain amounts of 25 dBR (defined as 10 $\log_{10}$ R), which is equivalent to 300 mm. However, the thunderstorm case shows these peaks being localized generally to areas in the interior of the southern Florida peninsula. The Irene case has large rain amounts covering the entire southern tip of the peninsula as well as covering the Florida Keys and extending out over the Atlantic Ocean. The localized peak rainfall cores in the thunderstorm case are primarily associated with the location of convective cores that last for time scales on the order of 1 h. The broad coverage of heavy rainfall in the hurricane case reflects the fact that the eyewall and stratiform rainfall covers a large area that spends considerable time (in this case 12 h) over the peninsula. The length of time a TC spends over a given location, which largely determines the total rainfall produced, is dependent on the size of the rainfall shield and translational speed of the storm.

PROCESSES THAT MODULATE TC RAINFALL DISTRIBUTIONS

The discussion above has generally described the radial distribution of rainfall in TCs, which essentially focuses on the axisymmetric rainfall structure. There are, however, many processes that can lead to the departure of TC rain fields from axisymmetry. Because of the strong tangential flow in TCs, these departures from axisymmetry often take the form of azimuthal asymmetries. However, other factors can create variations in the rainfall fields that are not circular in nature. The primary physical processes leading to TC rainfall asymmetries are topography, storm motion, vertical shear of the environmental wind, and interaction with midlatitude baroclinic systems/extratropical transition (ET).

The impact of topography on TC rainfall is primarily caused by flow being mechanically forced up the topographic barrier, leading to upward motion, destabilization, and rainfall on the windward side of the barrier (Figure 9). The degree to which topography enhances the rainfall is dependent on many factors, such as the structure and the intensity of the storm winds, the fetch of the winds, the incidence angle of the flow on the barrier, temperature and moisture content of the boundary layer flow, and the altitude at which the topographic lifting occurs (Smith and

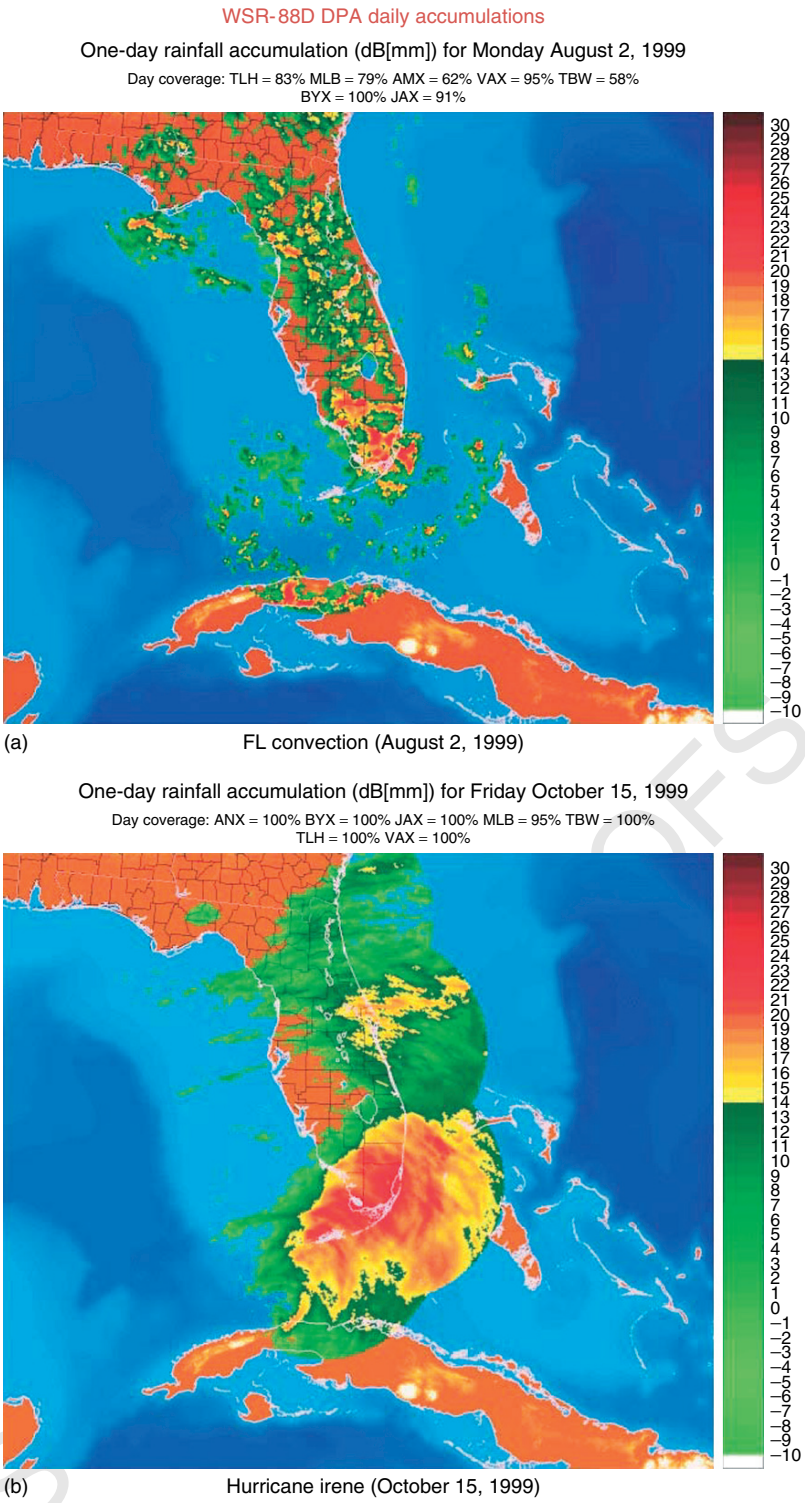

Figure 8 Daily accumulation of rainfall expressed in log(R) (d$BR = 10 \times \log_{10} R$) derived from WSR-88D observations for (a) August 2, 1999 and (b) October 15, 1999

Barstad, 2004; Lonfat *et al.*, 2007). Although all of these parameters are important, Alpert and Shafir (1989) show that the topographic ascent is the most important parameter to consider and Sinclair (1994) states that rainfall almost linearly depends on the surface wind, at first approximation. TCs impacting mountainous islands (e.g. Taiwan,

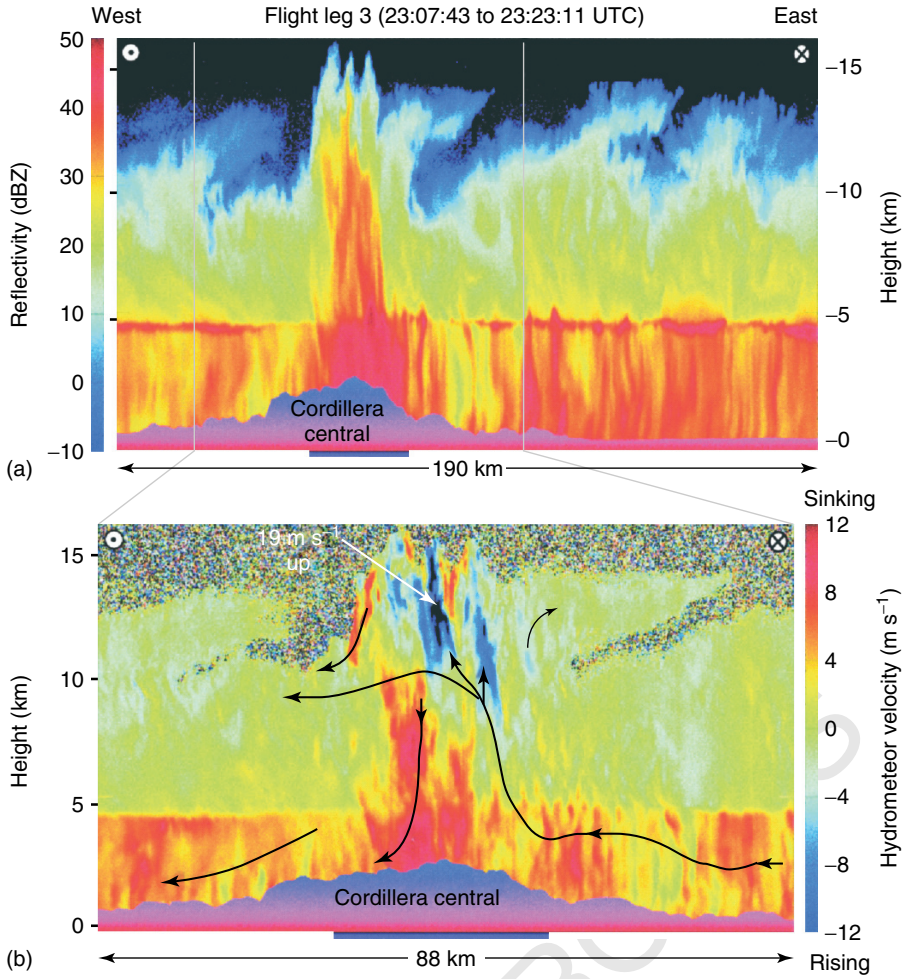

Figure 9 Nadir radar reflectivity (a; dBZ) from Doppler radar measurements from the NASA ER-2 aircraft in Hurricane Georges for time period 23:07–23:23 UTC September 22, 1998, when it interacts with the topography of Hispaniola. (b) Nadir Doppler velocity (shading, millimeter per second) and relative flow of air through the storm (arrows). (From Geerts *et al.* (2000). Reproduced by permission of American Meteorological Society)

Hispaniola, La Réunion) have been known to produce some of the most copious amounts of rainfall in the world (e.g. Figure 10; Lin *et al.*, 2002; Chiao and Lin, 2003). World records for TC rainfall totals (Table 1) all occurred at La Réunion, associated with the passage of TCs across this mountainous island in the southern Indian Ocean.

Storm motion is another factor that leads to asymmetries in TC rainfall. Several studies have documented this relationship (Powell, 1982; Shapiro, 1983; Bender, 1997; Corbosiero and Molinari, 2003; Lonfat *et al.*, 2004; Chen *et al.*, 2006), which has been attributed to azimuthal asymmetries in surface friction associated with peak surface winds located in the front-right quadrant relative to storm motion. The maximum inflow angle and boundary layer convergence are found in this quadrant, with the exact location dependent on the translational speed of the storm. For slow-moving storms ($<5\,\mathrm{m\,s^{-1}}$), the maximum convergence is located in a broad arc ahead of the storm, while for faster moving storms ($>10\,\mathrm{m\,s^{-1}}$) the convergence rotates clockwise and is concentrated in the right-front quadrant (left-front quadrant in the Southern Hemisphere). The net result on the distribution is to produce an azimuthal asymmetry, generally located in the front quadrant relative to storm motion (Figure 11).

Another process that has received considerable attention in recent years for its impact on creating azimuthal asymmetries in TC rainfall is the vertical shear of the environmental wind. Shear, generally considered between 850 and 200 hPa, is also associated with azimuthal asymmetries in the vertical motion and convergence fields. Several studies have shown that inner-core convection and rainfall tends to become organized on the left-hand side of the shear

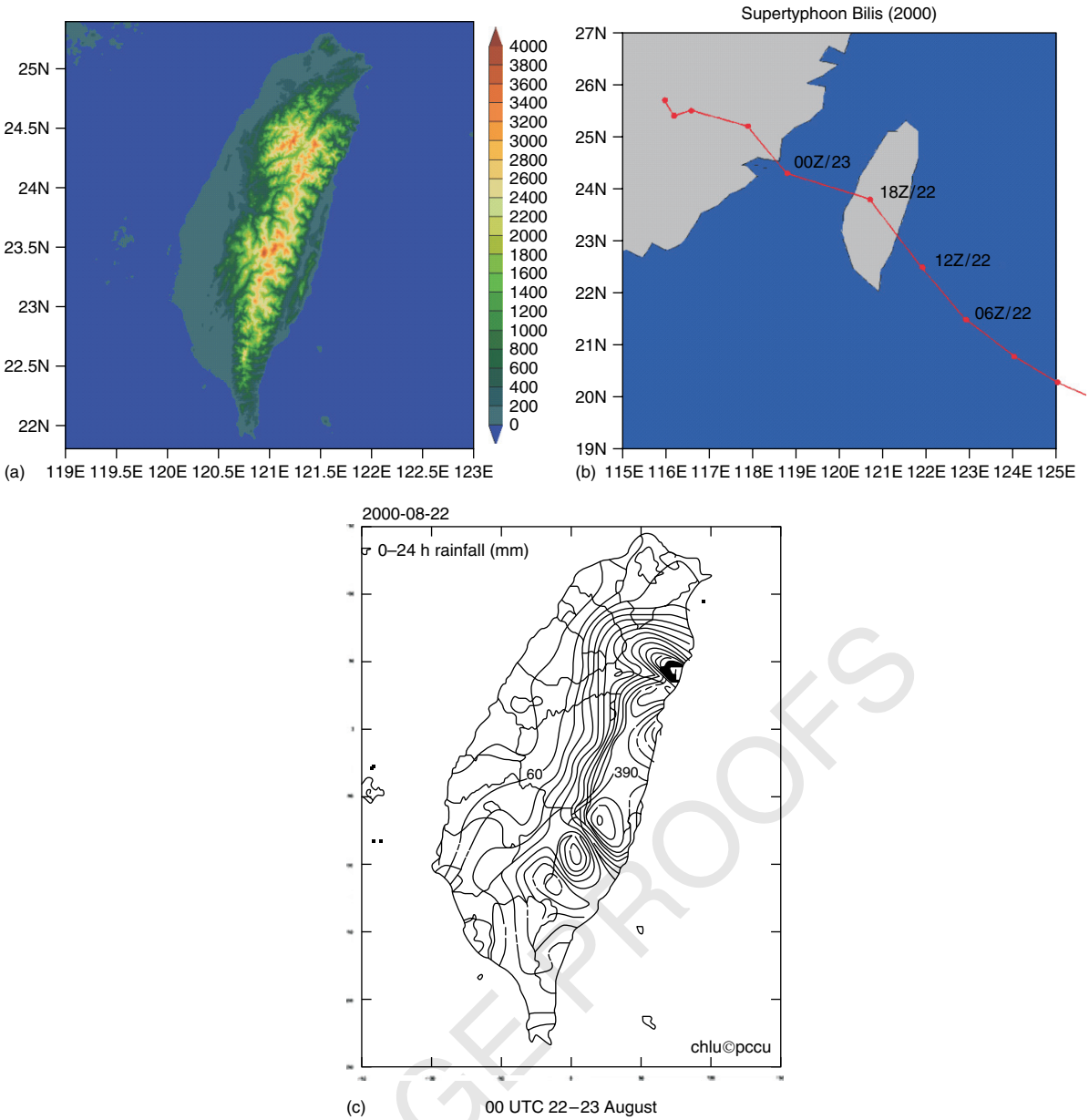

Figure 10 (a) Terrain height (meter) of Taiwan; (b) track of Supertyphoon Bilis from 00 UTC August 22 to 00 UTC August 24, 2000; and (c) 24-h rainfall totals (millimeter) from 00 UTC August 22 to 00 UTC August 23, 2000. (From Lin *et al.* (2002). Reproduced by permission of American Meteorological Society)

Table 1 World records for TC rainfall

Time period	Amount	Location	Storm	Date
12 h	1144 mm (45.0″)	Foc-Foc, La Reunion Island	Tropical Cyclone Denise	January 7–8, 1966
24 h	1825 mm (71.8″)	Foc-Foc, La Reunion Island	Tropical Cyclone Denise	January 7–8, 1966
72 h	3240 mm (127.6″)	Grand-Ilet, La Reunion Island	Tropical Cyclone Hyacinthe	January 24–27, 1980
10 days	5678 mm (223.5″)	Commerson, La Reunion Island	Tropical Cyclone Hyacinthe	January 18–27, 1980

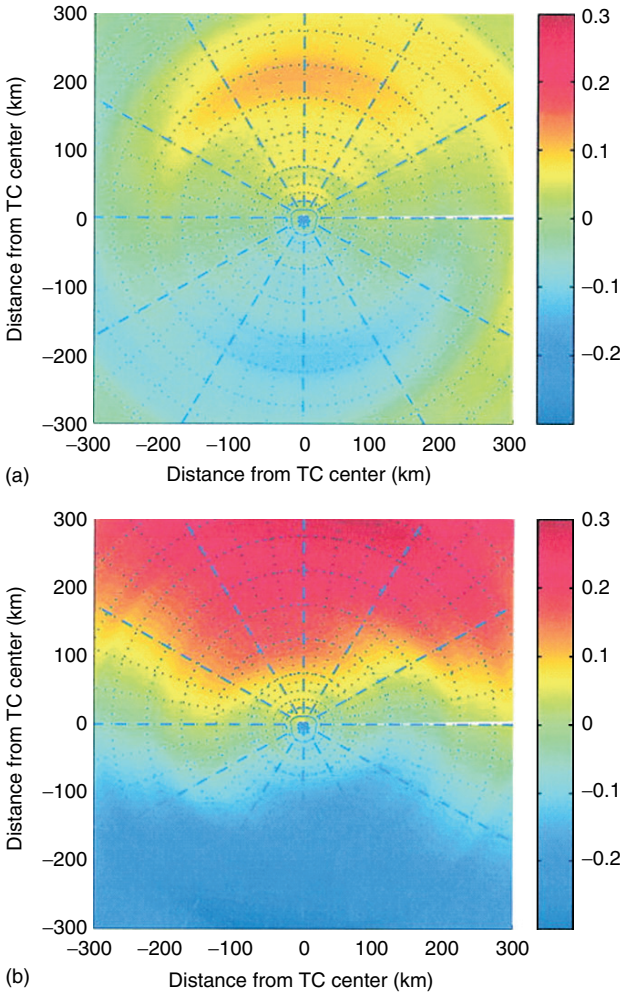

Figure 11 Rainfall asymmetry as a function of the storm translation speed: (a) $<5\,m\,s^{-1}$ and (b) $= 5\,m\,s^{-1}$. Storm motion is toward the top of the figure. The color scale represents the fraction of the wavenumber-1 asymmetry normalized by the azimuthal mean value. (Adapted from Lonfat *et al.* (2004). Reproduced by permission of American Meteorological Society)

vector when looking downshear for storms in the Northern Hemisphere (Figure 12; Willoughby *et al.*, 1984; Marks *et al.*, 1992; Franklin *et al.*, 1993; Frank and Ritchie, 1999; Black *et al.*, 2002; Corbosiero and Molinari, 2003; Chen *et al.*, 2006; Cecil, 2007). The conceptual model that has arisen from these studies is that updrafts are initiated downshear, near the location of the low-level inflow maximum. The updrafts are wrapped cyclonically around the core by the rapidly rotating tangential winds and create a maximum vertical motion in the downshear left quadrant (Figure 13). Maximum precipitation is displaced farther counterclockwise through advection, that is, in the 45–50 dBZ zone, as shown in Figure 13. The impact of vertical shear on the magnitude of the asymmetry is dependent on both the magnitude of the shear and the storm intensity. Figure 14 shows the amplitude of the wavenumber-1 coefficient describing the impact of shear on rainfall asymmetries as a fraction of the wavenumber-0 coefficient, based on observational data (Chen *et al.*, 2006). All plots show the downshear-left location of the peak in the rainfall asymmetry, but there are differences as a function of shear magnitude and storm intensity. For weaker shear values ($<5\,m\,s^{-1}$ between 850 and 200 hPa), the amplitude of the azimuthal asymmetry for tropical storms is much higher than that for major hurricanes. For stronger shear values ($>7.5\,m\,s^{-1}$), the asymmetry is still stronger for weaker systems, but the difference in amplitude is not as pronounced.

The above studies focus on the instantaneous distribution of rainfall (e.g. radar reflectivity) as a function of vertical shear. However, the accumulated rainfall distributions are dependent on both the vertical shear and the storm motion. When the vertical shear is oriented perpendicular to the track of the storm, the rainfall asymmetry accumulates symmetrically across the storm track (Figure 15; Rogers *et al.*, 2003). By contrast, when the shear is oriented parallel to the storm track, the rainfall asymmetry is concentrated on the left-hand side of the storm track, creating an accumulated rainfall maximum to the left of the track.

The interaction of TCs with baroclinic systems and their transition to extratropical status (ET) are also processes that can produce asymmetries in the rain field of TCs moving poleward. Strong flow ahead of the storm that interacts with frontal boundaries can produce uplift and torrential rainfall in much the same way as topographical barriers can. TCs undergoing ET typically experience strong vertical shear, leading to the development of pronounced azimuthal asymmetries (Jones *et al.*, 2003; Colle, 2003; Atallah and Bosart, 2003). Often these asymmetries extend several hundred kilometers ahead of the TC (Figure 16). Rainfall well in advance of these TCs can sometimes cause significant death and damage, as was the case in Hurricane Floyd (1999) (Lawrence *et al.* 2001).

TC RAINFALL FORECASTING METHODOLOGIES

While significant improvements have been made in forecasts of TC track (Franklin *et al.*, 2003; Aberson, 2001) and, to a lesser extent, intensity (DeMaria and Gross, 2003; DeMaria *et al.*, 2005), much less attention has been focused on improving forecasts of rainfall (quantitative precipitation forecasting or QPF) from TCs. With all of the processes that govern both the symmetric and the asymmetric distributions of TC rainfall described above, obtaining reliable TC QPF is a challenge. Various TC QPF schemes have been developed that address these processes to varying degrees. The simplest technique, which is known as *Kraft's rule of*

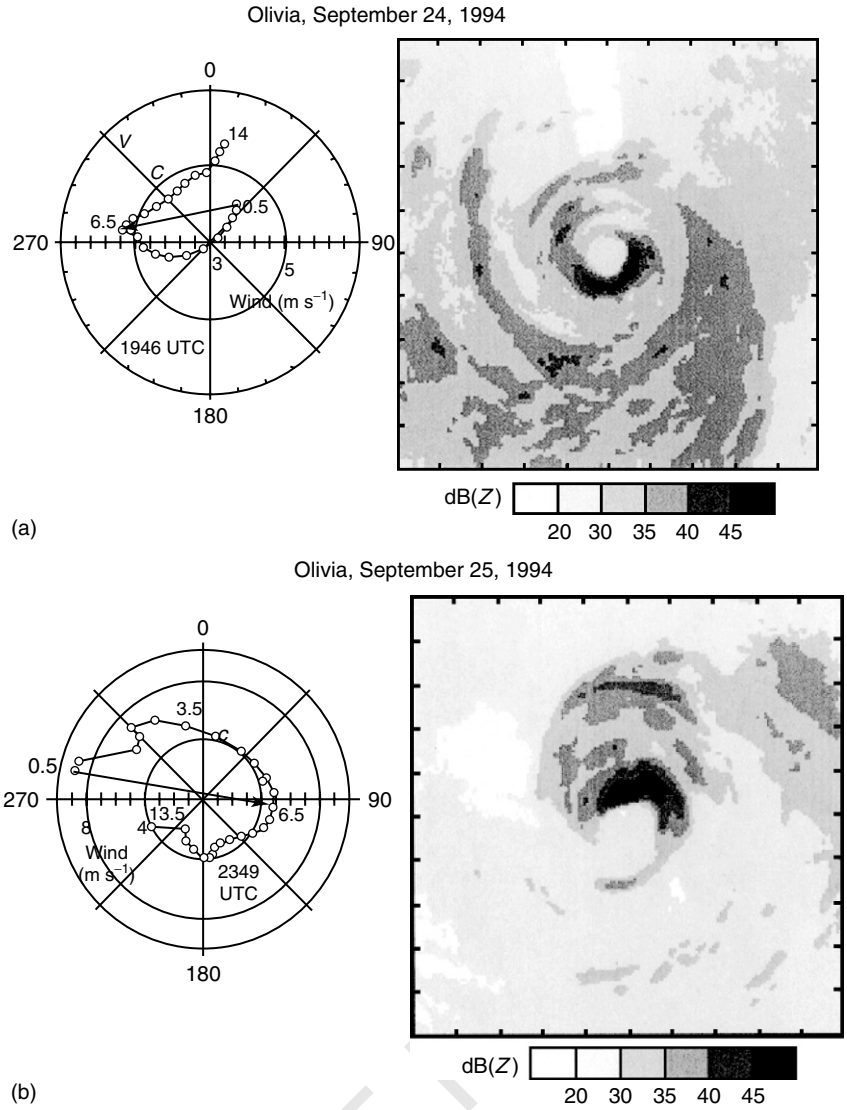

Figure 12 (a) Doppler-determined hodograph (left panel) of the storm-relative wind at 1946 UTC 24 September determined from airborne dual-Doppler wind synthesis. The arrow indicates the largest lower tropospheric shear. Letters C and V represent the storm motion and the vertically averaged wind, both expressed in a reference frame fixed to the earth. A 240 km × 240 km square composite of lower fuselage radar reflectivity for 1931–1951 UTC is also shown (right panel). (b) Doppler-determined relative-wind hodograph, storm motion, and earth-relative vertically averaged wind (left panel) at 23 : 49 UTC 25 September. Lower fuselage radar composite shown for 23 : 38–23 : 59 UTC (right panel). (From Black *et al.* (2002). Reproduced by permission of American Meteorological Society)

thumb (attributed to R.H. Kraft by Pfost (2000)), consists of dividing a constant value by the translational speed of the storm to estimate the maximum rainfall that will be produced over a given location and time period traversed by the storm. While this technique accounts for the translational speed of the storm, it includes no information on the structure of the rainfall field.

Other methods use observations of the current distribution of TC rainfall to generate short-term predictions of rainfall. One example is the tropical rainfall potential (TRaP) method (Kidder *et al.*, 2005), which translates a satellite-estimated precipitation field with the current storm motion to generate a 24-h rainfall accumulation (Figure 17). The advantages of this technique are that it runs relatively quickly and it incorporates all of the information about rainfall asymmetries. Because it assumes a steady-state rain field, however, this technique is really valid only for relatively short-term (e.g. <24 h) rainfall forecasts.

The rainfall climatology and persistence (R-CLIPER) model is a climatology-based parametric model that has recently been developed (Marks *et al.*, 2002; DeMaria and Tuleya, 2001; Tuleya *et al.*, 2007) to provide a benchmark

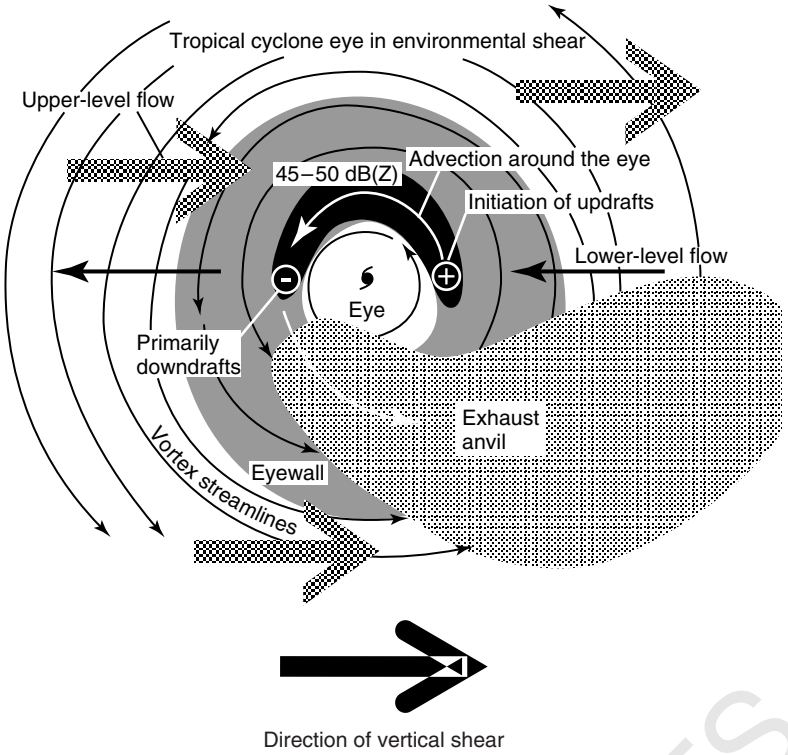

Figure 13 Schematic illustration of the shear-induced convective asymmetry based upon observations of Hurricanes Jimena and Olivia. The low-level environmental flow is indicated by the two solid black arrows. Upper-level flow is indicated by the three stippled arrows. Convective cells form somewhat upwind of the downshear side of the eyewall. They advect around the eye into the semicircle to the left of the shear vector where warm rain processes generate hydrometeors large enough to reflect radar effectively. Precipitation-driven downdrafts begin about 90° to the left of the shear vector. By the time the cells reach the upshear side of the eyewall they have ascended through the 0 °C isotherm and downdrafts predominate below 6 km. As the cells move into the semicircle on the right of the shear vector, most condensate freezes or falls out of the active updrafts. The unloaded updrafts accelerate upward. They detach from the eyewall and approach the tropopause as they rotate through the semicircle to the right of the shear. (From Black *et al.* (2002). Reproduced by permission of American Meteorological Society)

against which forecasts of TC rainfall can be compared, similar to the way in which climatology and persistence-based CLIPER (Neumann, 1972; Aberson, 1998) and statistical hurricane intensity forecast SHIFOR (Jarvinen and Neumann, 1979; Knaff *et al.*, 2003) model predictions provide the benchmarks for track and intensity forecasts, respectively. The current operational version of the R-CLIPER, which is based on satellite-derived TC rainfall observations (Marks *et al.*, 2002), assumes a circularly symmetric distribution of rainfall and translates this distribution in time. It captures the dominant signals of translational speed and storm intensity, but it does not incorporate other processes that create asymmetries in the rain field. To account for at least some of these asymmetries, a new parametric model called the *parametric hurricane rainfall model* (*PHRaM*) was developed to account for the effects of vertical shear and topography on TC rainfall fields (Lonfat *et al.*, 2007). PHRaM is based on the R-CLIPER model, with the addition of an azimuthal Fourier decomposition to account for shear and a term proportional to the change in elevation of parcels moved every 15 min to replicate the impacts of topographical uplift. Comparisons of PHRaM rainfall forecasts with those using the standard version of R-CLIPER show significantly improved rainfall fields, in particular, in areas where the TC interacts with topography (Figure 18). Another parametric model has recently been developed that accounts for storm motion and intensity, vertical shear of the environmental wind, and various assumed characteristics of the TC boundary layer that compares well with tropical rainfall measuring mission (TRMM) satellite measurements and high-resolution numerical model simulations of rainfall distributions (Langousis and Veneziano, 2009).

The most complex forecasting systems for producing TC QPF are three-dimensional numerical models that produce spatially and temporally varying rainfall fields. The benefit of using numerical models is their ability to depict changes in the structure of TCs over time and how these changes are reflected in the rain field, both in a storm-relative sense and with accumulated rainfall swaths over a

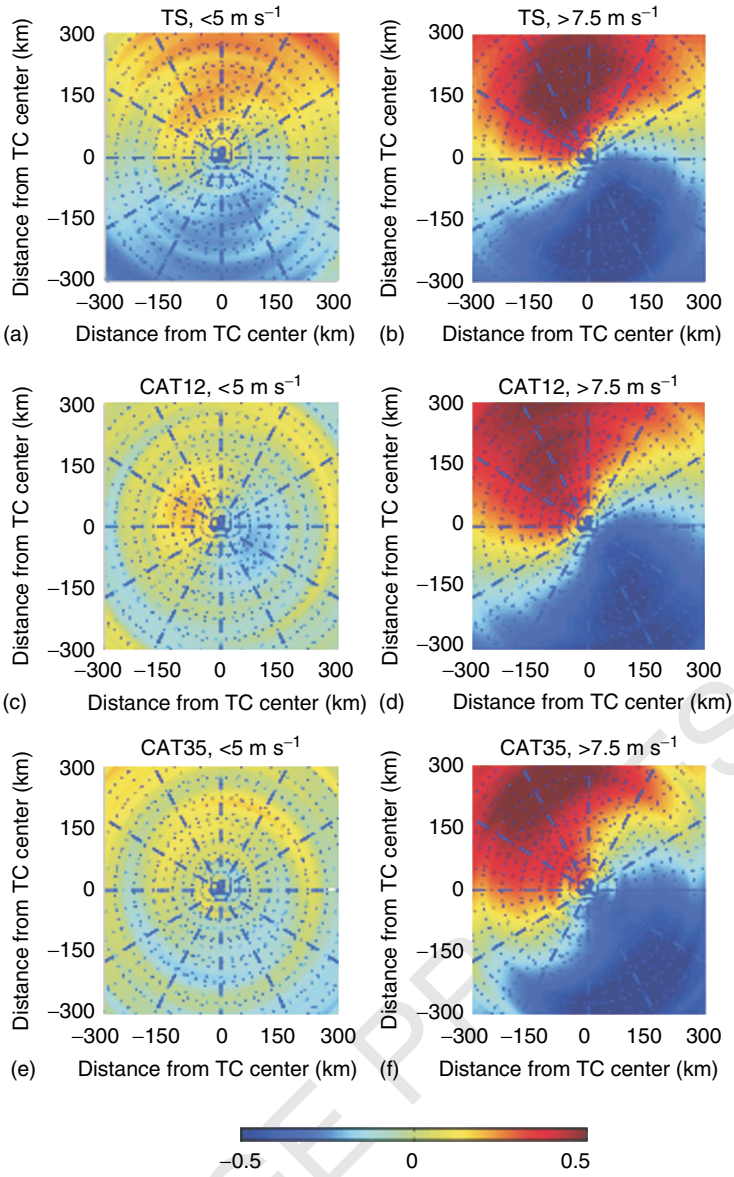

Figure 14 The wavenumber-1 rainfall asymmetry relative to the 200- to 850-hPa environmental vertical wind shear for various storm intensities and shear magnitudes: (a) tropical storm strength, shear $<5\,m\,s^{-1}$; (b) tropical storm strength, shear $>7.5\,m\,s^{-1}$; (c) category 1–2 hurricane, shear $<5\,m\,s^{-1}$; (d) category 1–2 hurricane, shear $>7.5\,m\,s^{-1}$; (e) category 3–5 hurricane, shear $<5\,m\,s^{-1}$; and (f) category 3–5 hurricane, shear $>7.5\,m\,s^{-1}$. The analysis is done in a cylindrical coordinate. The shear vector is pointed to the top in all panels. The color scale represents the fraction of the wavenumber-1 asymmetry normalized by the azimuthal mean value. (Adapted from Chen *et al.* (2006). Reproduced by permission of American Meteorological Society)

geographical area. These models have different initialization schemes, resolutions, and physical parameterizations, which can produce significant differences in their rainfall forecasts. For example, Figure 19 shows 72-h accumulated rainfall fields for Hurricane Isabel (2003) produced by four models geophysical fluid dynamics laboratory (GFDL), global forecasting system (GFS), north American mesoscale (NAM), and R-CLIPER that have varying resolution and complexity, compared with observations (Marchok *et al.*, 2007). The observed rain maximum (Figure 19a) stretches along and just to the right-hand side of the storm track, and there is significant structure in the rain field, corresponding to rainbands and topographic effects. Although the R-CLIPER reproduces the general pattern of rainfall, the amounts are smaller than observed and not much of the structure in the rain field is predicted. The GFDL predicts

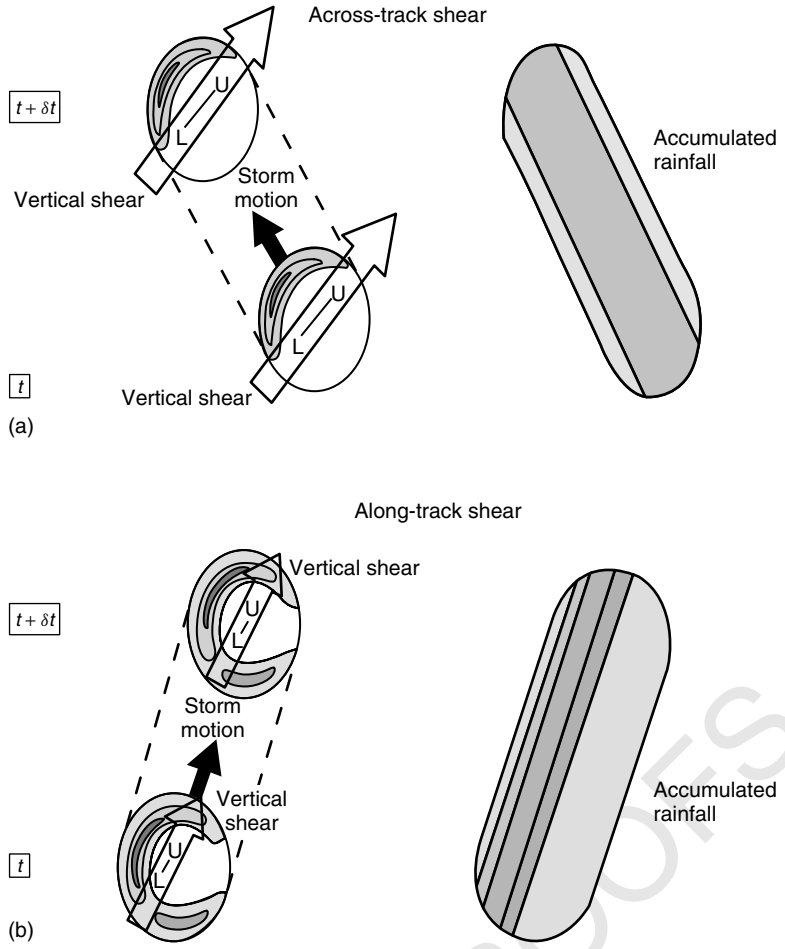

Figure 15 Simplified schematic showing relationships between shear, storm heading, vortex tilt, instantaneous rainfall (reflectivity), and total rainfall. Shading in left column denotes reflectivity; increasingly dark shading indicates increasingly high reflectivity (i.e. rain rates). Shading in right column denotes total accumulated rainfall during δt time period; increasingly dark shading indicates increasingly heavy total rainfall amounts. Symbols L and U in left column denote locations of lower- and upper-level vortex centers, respectively. Thick solid arrow in left column indicates storm heading; thick transparent arrow in left column indicates vertical wind shear vector. (a) Across-track shear and (b) along-track shear. (From Rogers *et al.* (2003). Reproduced by permission of American Meteorological Society)

rain amounts and structures comparable to the observations, and the NAM and GFS predict some structure to the rain field. Although the GFS predicts a larger area of maximum rain than was observed, the NAM predicts a smaller area of the heavy rain. Farther inland over Ohio and West Virginia, the GFDL and NAM models, and to a lesser extent the GFS model, predict a secondary axis of heavier rainfall to the left of the observed storm track that is consistent with the observations. However, the R-CLIPER produces only the main axis of heaviest rainfall that is aligned with the storm track.

The differences shown in the example above can be quantified statistically by considering TC QPF performance for many storms over many years. Marchok *et al.* (2007) compared the performance of these models for all US landfalling storms from 1998 to 2004. An example of one such comparison is shown in Figure 20. This figure shows probability distribution functions (PDFs) of rain flux, which is simply the product of the rainfall value at a grid point and the representative areal coverage of that point. The PDF of rain flux for the GFDL, NAM, and observed rainfall fields for the 0- to 100-km band around the storm track (Figure 20a), where rainfall from the eyewall (or eyewall remnants) would tend to predominate, shows that the GFDL has a clear tendency to produce too much rain flux in the high-to-extreme rain amounts, while the NAM produces too much rain flux in the light-to-moderate rain amounts. This suggests that the GFDL tends to overestimate heavy (convective) rain, while the NAM tends to underestimate heavy (convective) rain. The GFS and R-CLIPER comparisons in this swath (Figure 20b) show that the GFS slightly overestimates

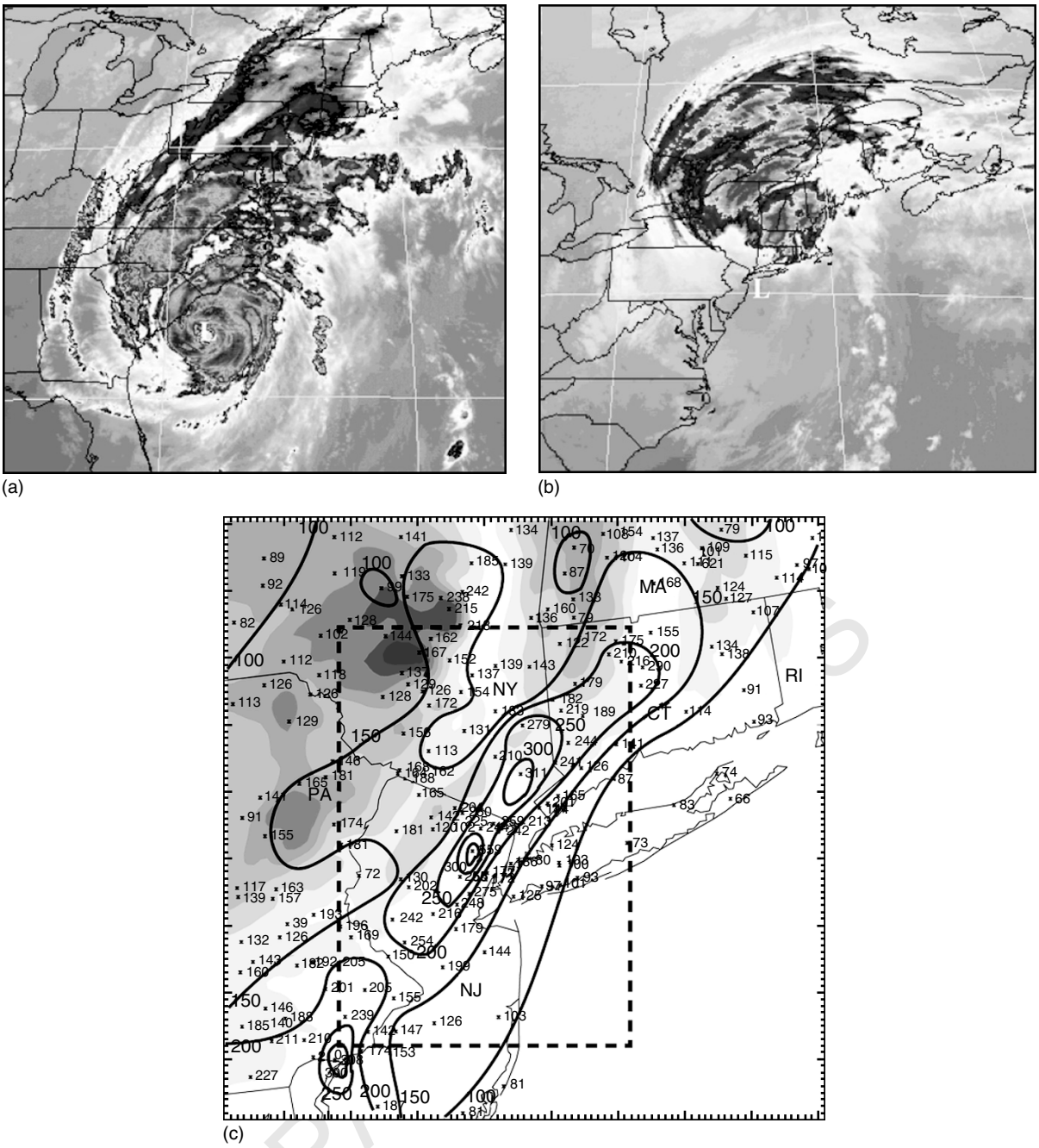

Figure 16 Infrared satellite images for (a) 00 : 00 UTC September 16, 1999 and (b) 00 : 00 UTC September 17, 1999. The center of Floyd is labeled with a white L. (c) Observed precipitation (solid every 50 mm) from 06 : 00 UTC September 16, 1999 to 06 : 00 UTC September 17, 1999. Terrain is shaded every 150 m starting at 100 m. (Adapted from Colle (2003). Reproduced by permission of American Meteorological Society)

rain flux for moderate to heavy (convective) rain amounts (<10 in (254 mm)), but it underestimates rain flux for the extreme rain amounts (>10–15 in (254–381 mm)). The R-CLIPER has the closest resemblance to the observed flux distributions in the inner core (Figure 20b), showing the ability to produce rain flux that matches the observed for light, moderate, heavy, and extreme rain amounts. The corresponding rain flux PDFs for the 300–400 km swath, where a mixture of rainband and stratiform rain would likely predominate, are shown in Figure 20(c) and (d). The rain flux PDF from the GFDL model (Figure 20c) agrees well with the observations in this swath. The GFS

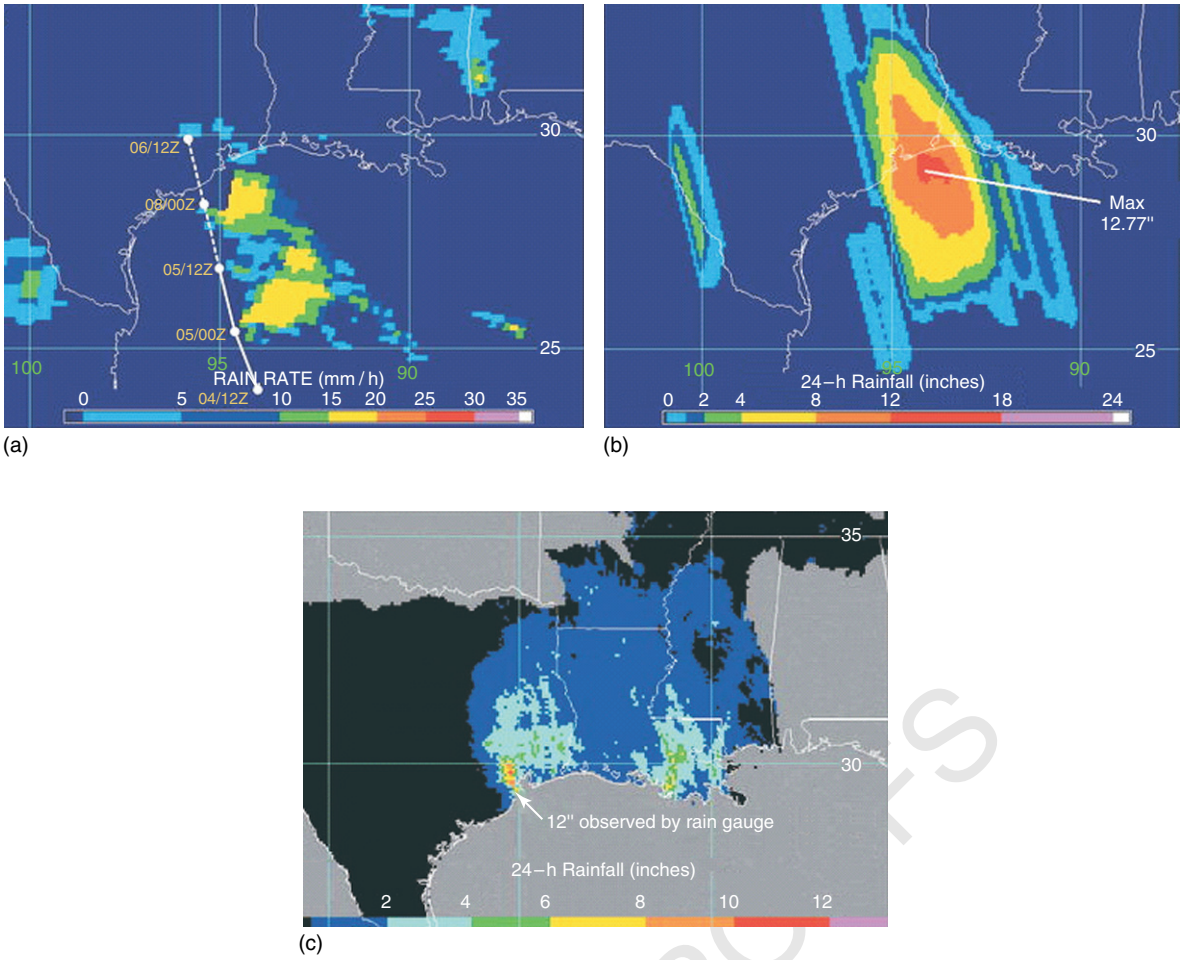

Figure 17 (a) NOAA-16 AMSU-B rain rates for Tropical Storm Allison at 08:12 UTC on June 5, 2001. (b) The 24-h TRaP for the period ending 12:00 UTC on June 6, 2001. (c) Stage III rain gauge-adjusted radar rainfall estimates for the 24-h period ending at 12:00 UTC on June 6, 2001. (Adapted from Kidder *et al.* (2005). Reproduced by permission of American Meteorological Society)

(Figure 20d) shows a slight tendency to overestimate rain flux for the stratiform amounts and to underestimate rain flux for the heavy (convective) rain amounts. Although the R-CLIPER 0- to 100-km rain flux PDF agrees very well with the observations, the 300- to 400-km rain flux PDF is significantly skewed toward lighter rain rates. That is, the R-CLIPER significantly overestimates rain flux for the light rain amounts in the 300- to 400-km swath and significantly underestimates rain flux for the moderate-to-heavy rain amounts.

SUMMARY AND OUTLOOK

Rainfall is one of the most significant impacts of landfalling TCs. It is responsible for a significant proportion of the loss of life and property from TCs. Despite this, some beneficial impacts accompany rainfall from TCs, including the significant contribution that TC rainfall makes to total rainfall in some parts of the globe. In some regions, TC rain is a significant portion of the yearly total and, therefore, an important source of fresh water. For these reasons, improved understanding and prediction of TC rainfall are of high importance.

The sources of TC rainfall can be grouped into three primary structures: the eyewall, which consists primarily of convective rainfall; the rainbands, which can consist of a combination of convective and stratiform rainfall; and stratiform rain. Precipitation in the eyewall is usually the most intense, as it is associated with broad upward motion in the ascending branch of the cyclone's secondary circulation with embedded convective elements. By contrast, stratiform precipitation, generally fed by hydrometeors detrained from convection in the eyewall and rainband regions, is usually the lightest. However, the areal coverage of the stratiform region is much larger than the eyewall, so the stratiform areas can produce as much total rainfall as the eyewall.

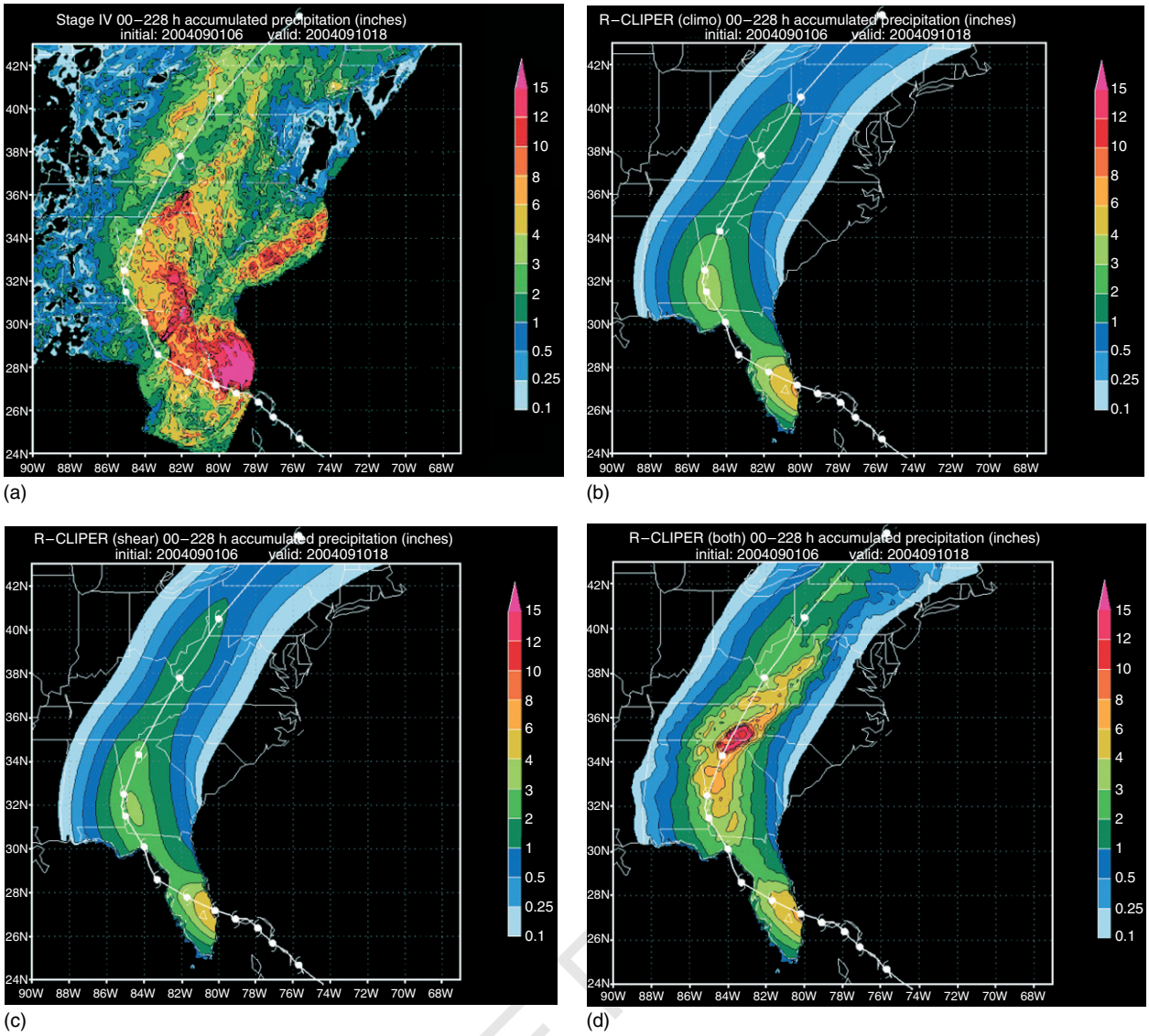

Figure 18 Rainfall accumulations (in) for a 9.5-day time period (06 UTC September 1–18 UTC September 10, 2004) corresponding to the path of Hurricane Frances over the eastern Seaboard. (a) Stage-IV gauge-corrected radar observations; (b) rainfall-CLIPER (R-CLIPER) run; (c) R-CLIPER run with vertical shear included; and (d) R-CLIPER run with vertical shear and topography included (i.e. PHRaM)

Hydrometeors in the stratiform regions can be advected several times around the cyclone in the strong tangential flow as they slowly descend back to the ground. In the mean, peak inner-core rainfall is most intense for strong TCs and least intense for tropical storms. These differences vanish at larger radii (i.e. 250 km).

Many processes contribute to generate asymmetries in the rainfall fields from TCs. The primary processes are interactions with topography, storm motion, and vertical shear and interactions with midlatitude features such as frontal boundaries. Topography has been responsible for producing some of the heaviest rainfall events in the world. Storm motion generally leads to an area of low-level convergence and rainfall in the front-right quadrant. Vertical shear creates convergence and low-level upward motion in the downshear quadrant that leads to a rainfall maximum on the downshear-left (in the northern hemisphere) side of the storm. Interactions with midlatitude features and ET can also create copious rainfall amounts, especially far ahead of the track of the storm.

Techniques for forecasting TC rainfall range from simple relationships using the storm translational speed to parametric models to fully three-dimensional numerical models. Each of the schemes has its benefits and drawbacks; the simpler schemes benefit from the ease of running them at the cost of incorporating complexities in the rainfall

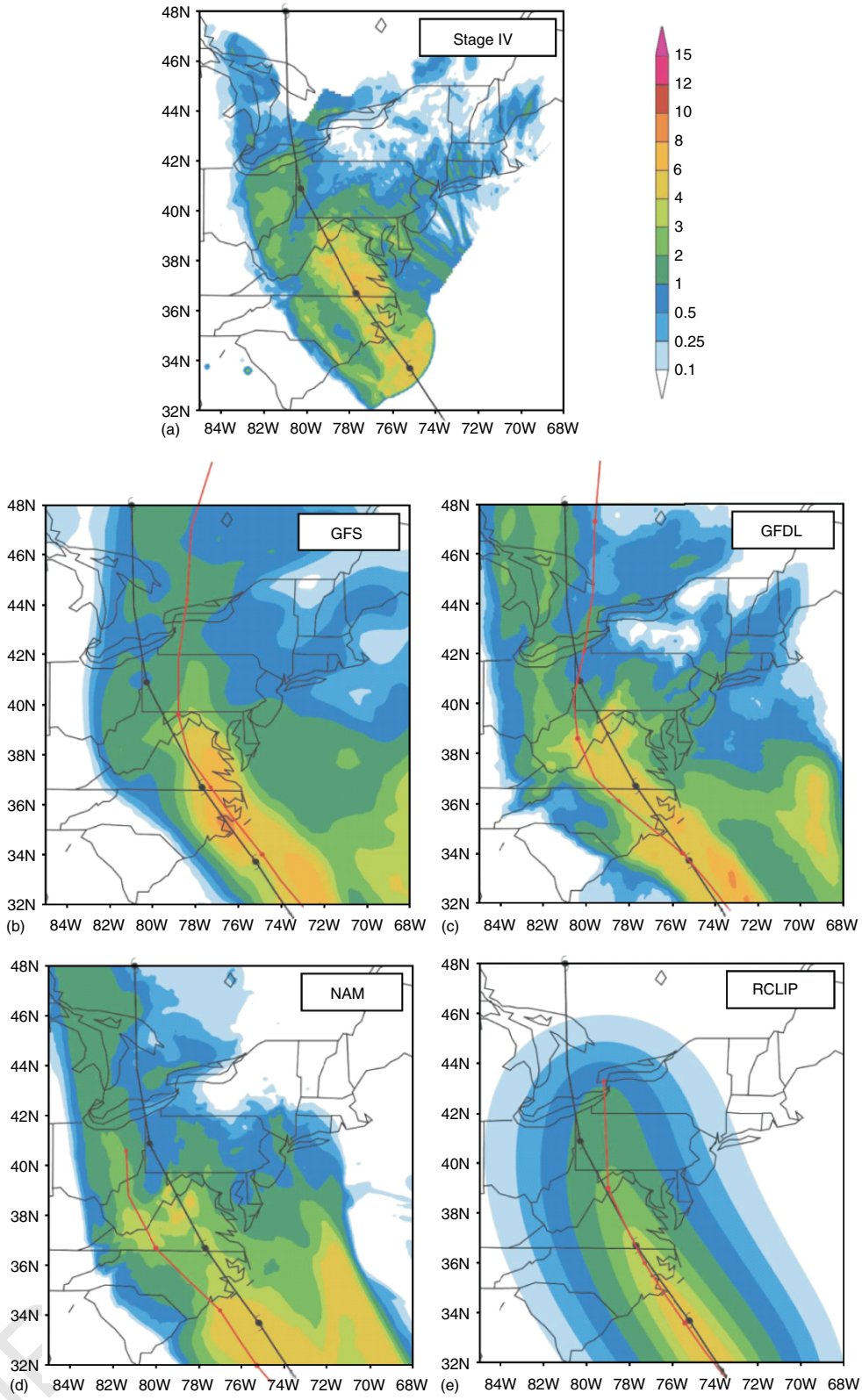

Figure 19 Plot of 72-h accumulated rain (shaded, inches) from 12:00 UTC September 17 to 12:00 UTC September 20, 2003 for (a) stage-IV observations, (b) GFS, (c) GFDL, (d) NAM, and (e) R-CLIPER. The observed track is shown in black; each model's forecast track is shown in red. (From Marchok *et al.* (2007). Reproduced by permission of American Meteorological Society)

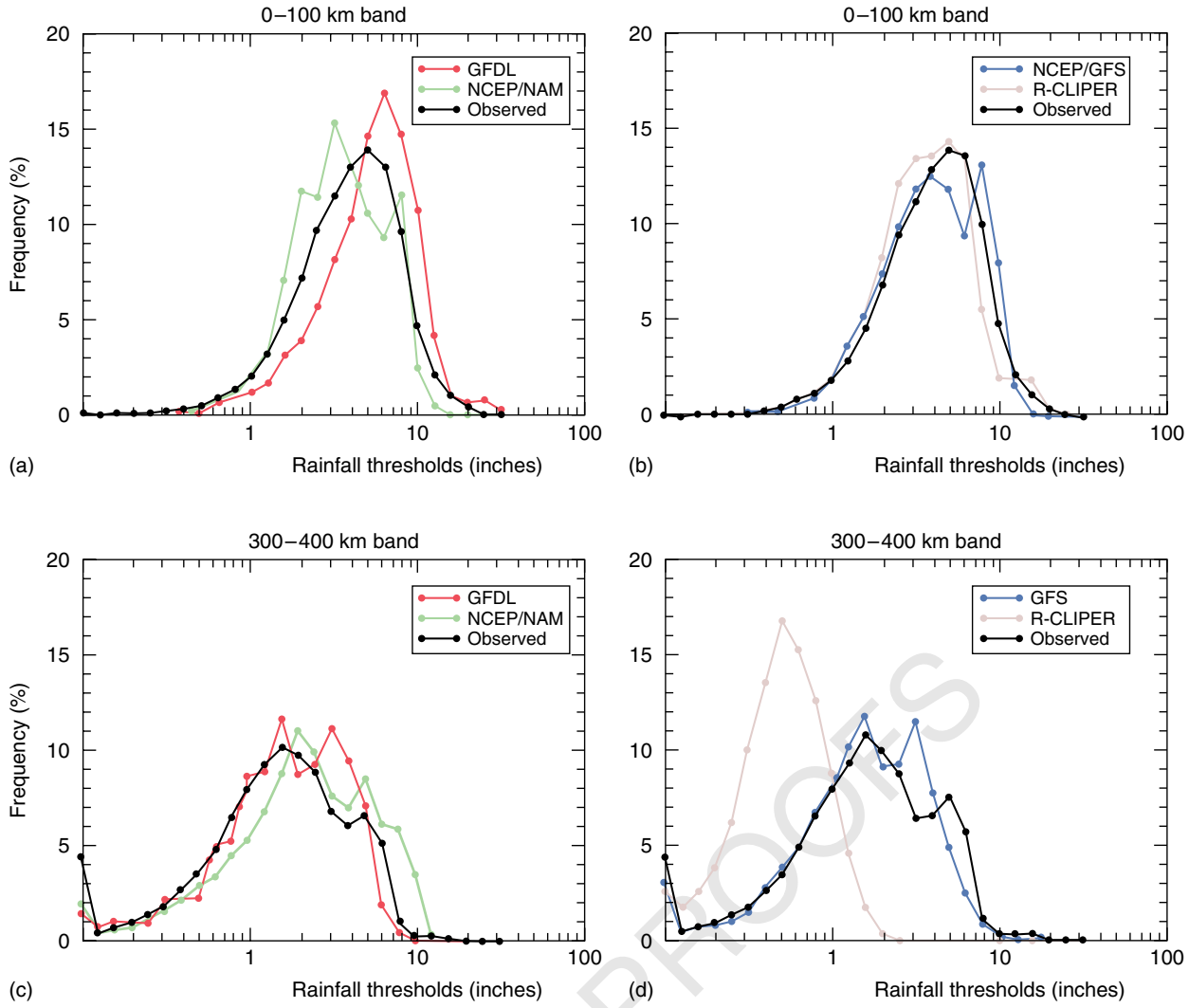

Figure 20 Probability distribution functions (PDFs) of rain flux for all models and observations for all US landfalling tropical cyclones from 1998 to 2004. (a) PDFs of rain flux within 0 to 100-km track-relative swath for GFDL, NAM, and stage IV. (b) As in (a) but for GFS, R-CLIPER, and stage IV. (c) PDFs of rain flux within 300- to 400-km track-relative swath for GFDL, NAM, and stage IV. (d) As in (c) but for GFS, R-CLIPER, and stage IV. (From Marchok *et al.* (2007). Reproduced by permission of American Meteorological Society)

fields. The more complex schemes are better able to depict asymmetries in the rainfall fields, but they too suffer from deficiencies stemming from the inadequate representation of the initial conditions, insufficient horizontal and vertical resolutions, and deficient representation of the physical processes in the model.

Future work in TC rainfall can be divided into forecasting and research activities. On the forecasting side, improvements can always be made in the numerical models described above. As new operational forecast models come online, with more sophisticated physical parameterizations, improved techniques for initializing the TC vortex and environment, and higher resolution, the prospect for improved rainfall forecasts is clear.

More work is needed to rigorously evaluate rainfall from TC models, however, in order to properly identify possible biases in the models and target ways to improve them. Such model evaluations can follow traditional validation metrics for rainfall, such as equitable threat scores and bias scores, but new evaluation techniques that are better adapted to the unique qualities of TC rainfall and the observations that are collected in TCs (Marchok *et al.*, 2007; Rogers *et al.*, 2007) are needed as well. Additional work in parametric modeling is also promising. One possibility is to produce ensemble rainfall forecasts for parameters such as threshold rainfall values from a variety of forecasted storm tracks. The inclusion of additional processes such as ET in parametric models

may also improve forecasts of TC rainfall for particular events.

Research in TC rainfall can focus on a wide variety of topics. One area of interest focuses on how rainfall fields relate to TC structure and evolution. What is the role of convective versus stratiform processes in TC genesis and intensity change? What is the significance of precipitation processes compared to dynamical processes for TC genesis, intensity, and structural changes? Are there systematic differences in the structure of rainfall fields that can be measured, for example, from aircraft or satellites, which can provide some predictive ability for TC intensity and structural changes? Can these differences be represented by numerical models? To what extent do aerosol type and amount impact rainfall in TCs? On larger spatial and temporal scales, research is needed to better understand the feedback of TC rainfall on global and regional rainfall distributions and how these variations impact society. Such research is critical to improve our understanding and prediction not only of TC rainfall, structure, and evolution but also of the impacts of TC rainfall on society as a whole.

REFERENCES

Aberson S.D. (1998) Five-day tropical cyclone track forecasts in the North Atlantic basin. *Weather and Forecasting*, **13**, 1005–1015.

Aberson S.D. (2001) The ensemble of tropical cyclone track forecasting models in the North Atlantic Basin (1976–2000). *Bulletin of the American Meteorological Society* **82**, 1895–1904.

Alpert P. and Shafir H. (1989) Meso-scale distribution of orographic precipitation: numerical study and comparison with precipitation derived from radar measurements. *Journal of Applied Meteorology*, **28**, 1105–1117.

Atallah E.H. and Bosart L.F. (2003) The extratropical transition and precipitation distribution of Hurricane Floyd (1999). *Monthly Weather Review* **131**, 1063–1081.

Bender M.A. (1997) The effect of relative flow on the asymmetric structure in the interior of hurricanes. *Journal of the Atmospheric Sciences*, **54**, 703–724.

Black M.L., Gamache J.F., Marks F.D., Samsury C.E. and Willoughby H.E. (2002) Eastern Pacific Hurricanes Jimana of 1991 and Olivia of 1994: the effect of vertical shear on structure and intensity. *Monthly Weather Review*, **130**, 2291–2312.

Cecil D.J. (2007) Satellite-derived rain rates in vertically sheared tropical cyclones. *Geophysical Research Letters*, **34**, L02811, DOI:10.1029/2006GL027942.

Chen S.S., Knaff J.A. and Marks F.D. (2006) Effects of vertical wind shear and storm motion on tropical cyclone rainfall asymmetries deduced from TRMM. *Monthly Weather Review*, **134**, 3190–3208.

Chiao S. and Lin Y.L. (2003) Numerical modeling of an orographically enhanced precipitation event associated with tropical storm rachel over Taiwan. *Weather and Forecasting*, **18**, 325–344.

Colle B.A. (2003) Numerical simulations of the extratropical transition of Floyd (1999): structural evolution and responsible mechanisms for the heavy rainfall over the northeast United States. *Monthly Weather Review*, **131**, 2905–2926.

Corbosiero K.L. and Molinari J. (2003) The effects of vertical wind shear on the distribution of convection in tropical cyclones. *Monthly Weather Review* **130**, 2110–2123.

DeMaria M. and Gross J.M. (2003) Evolution of tropical cyclone forecast models. In *Hurricane! Coping with Disaster*, Simpson R. (Ed.), American Geophysical Union: pp. 103–126.

DeMaria M., Mainelli M., Shay L.K., Knaff J.A. and Kaplan J. (2005) Further improvements to the statistical hurricane intensity prediction scheme (SHIPS). *Weather and Forecasting* **20**, 531–543.

DeMaria, M. and Tuleya, R.E. (2001) *Evaluation of quantitative precipitation forecasts from the GFDL hurricane model*. Preprints, *Symposium on Precipitation Extremes: Prediction, Impacts, and Responses. 81st Annual Meeting of the AMS*, Albequerque, NM, American Meteorological Society, pp. 340–343.

Dodge P., Burpee R.W. and Marks F.D. (1999) The kinematic structure of a hurricane with sea level pressure less than 900 mb. *Monthly Weather Review*, **127**, 987–1004.

Frank W.M. and Ritchie E.A. (1999) Effects of environmental flow upon tropical cyclone structure. *Monthly Weather Review*, **127**, 2044–2061.

Franklin J.L., Lord S.J., Feuer S.E. and Marks F.D. (1993) The kinematic structure of hurricane gloria (1985) determined from nested analyses of dropwindsonde and doppler radar data. *Monthly Weather Review*, **121**, 2433–2451.

Franklin J.L., McAdie C.J. and Lawrence M.B. (2003) Trends in track forecasting for tropical cyclones threatening the United States, 1970–2001. *Bulletin of the American Meteorological Society*, **84**, 1197–1203.

Geerts B., Heymsfield G.M., Tian L., Halverson J.B., Guillory A. and Mejia M.I. (2000) Hurricane Georges's Landfall in the Dominican Republic: detailed airborne doppler radar imagery. *Bulletin of the American Meteorological Society*, **81**, 999–1018.

Jarvinen, B.R. and Neumann, C.J. (1979) *Statistical Forecasts of Tropical Cyclone Intensity for the North Atlantic Basin*. NOAA Tech. Memo. NWS NHC-10, 22. [Available from National Technical Information Service, 5285 Port Royal Rd., Springfield, VA 22161.].

Jones S.C., Harr P.A., Abraham J., Bosart L.F., Bowyer P.J., Evans J.L., Hanley D.E., Hanstrum B.N., Hart R.E., Lalaurette F. *et al.* (2003) The extratropical transition of tropical cyclones: forecast challenges, current understanding, and future directions. *Weather and Forecasting*, **18**, 1052–1092.

Jorgensen D.P. and Willis P.T. (1982) A Z-R relationship for Hurricanes. *Journal of Applied Meteorology*, **21**, 356–366.

Kidder S.Q., Kusselson S.J., Knaff J.A., Ferraro R.R., Kuligowski R.J. and Turk M. (2005) The tropical rainfall potential (TRaP) technique. part I: description and examples. *Weather and Forecasting*, **20**, 456–464.

Knaff J.A., DeMaria M., Sampson C.R. and Gross J.M. (2003) Statistical, 5-day tropical cyclone intensity forecasts derived from climatology and persistence. *Weather and Forecasting*, **18**, 80–92.

Knight D.B. and Davis R.E. (2007) Climatology of tropical cyclone rainfall in the southeastern United States. *Physical Geography*, **28**, 126–147.

Konrad, C.E. II and Perry, L.B. (2009) Relationships between tropical cyclones and heavy rainfall in the Carolina region of the USA. *International Journal of Climatology*, DOI:10.1002/joc.1894.

Langousis A. and Veneziano D. (2009) Theoretical model of rainfall in tropical cyclones for the assessment of long-term risk. *Journal of Geophysical Research*, **114**, D02106, DOI:10.1029/2008JD010080.

Lawrence M.B., Avila L.A., Beven J.L., Franklin J.L., Guiney J.L. and Pasch R.J. (2001) Atlantic hurricane season of 1999. *Monthly Weather Review*, **129**, 3057–3084.

Lin Y.L., Ensley D.B., Chiao S. and Huang C.Y. (2002) Orographic influences on rainfall and track deflection associated with the passage of a tropical cyclone. *Monthly Weather Review*, **130**, 2929–2950.

Lonfat M., Marks F.D. and Chen S.S. Jr. (2004) Precipitation distribution in tropical cyclones using the tropical rainfall measuring mission (TRMM) microwave imager: a global perspective. *Monthly Weather Review*, **132**, 1645–1660.

Lonfat M., Rogers R., Marchok T. and Marks F.D. (2007) A parametric model for predicting hurricane rainfall. *Monthly Weather Review*, **135**, 3086–3097.

Marchok T., Rogers R. and Tuleya R. (2007) Validation schemes for tropical cyclone quantitative precipitation forecasts: evaluation of operational models for U.S. landfalling cases. *Weather and Forecasting*, **22**, 726–746.

Marks F.D. (2003) State of the science: radar view of tropical cyclones. *Meteorological Monographs*, **30**, 33.

Marks F.D. and Houze R.A. (1987) Inner core structure of hurricane alicia from airborne doppler radar observations. *Journal of the Atmospheric Sciences*, **44**, 1296–1317.

Marks F.D., Houze R.A. and Gamache J.F. (1992) Dual-aircraft investigation of the inner core of hurricane Norbert. Part I: kinematic structure. *Journal of the Atmospheric Sciences*, **49**, 919–942.

Marks, F.D., Kappler, G. and DeMaria, M. (2002) Development of a tropical cyclone rainfall climatology and persistence (R-CLIPER) model. Preprints, 25th *Conference on Hurricanes and Tropical Meteorology*, San Diego, CA, American Meteorological Society, pp. 327–328.

Neumann, C.J. (1972) *An Alternate to the Hurran (Hurricane Analog) Tropical Cyclone Forecasting System*. NOAA Tech. Memo. NWS SR-62, 23. [Available from NTIS, Technology Administration, U.S. Department of Commerce, Springfield, VA 22161.].

Pfost R.L. (2000) Operational tropical cyclone quantitative precipitation forecasting. *National Weather Digest*, **24**, 61–66.

Powell M.D. (1982) The transition of the hurricane frederic boundary-layer wind field from the open Gulf of Mexico to Landfall. *Monthly Weather Review*, **110**, 1912–1932.

Rappaport E.N. (2000) Loss of life in the United States associated with recent Atlantic tropical cyclones. *Bulletin of the American Meteorological Society*, **81**, 2065–2074.

Rogers R.F., Black M.L., Chen S.S. and Black R.A. (2007) An evaluation of microphysics fields from mesoscale model simulations of tropical cyclones. Part I: comparisons with observations. *Journal of the Atmospheric Sciences*, **64**, 1811–1834.

Rogers R.F., Chen S.S., Tenerelli J.E. and Willoughby H.E. (2003) A numerical study of the impact of vertical shear on the distribution of rainfall in Hurricane Bonnie (1998). *Monthly Weather Review*, **131**, 1577–1599.

Saffir H.S. (1973) Hurricane wind and storm surge. *The Military Engineer*, **423**, 4–5.

Shapiro L.J. (1983) The asymmetric boundary layer flow under a translating hurricane. *Journal of the Atmospheric Sciences* **40**, 1984–1998.

Simpson, R.H. (1974) The hurricane disaster potential scale. *Weatherwise*, **27**, 169–186.

Sinclair M.R. (1994) A diagnostic model for estimating orographic precipitation. *Journal of Applied. Meteorology*, **33**, 1163–1175.

Smith R.B. and Barstad I. (2004) A linear theory of orographic precipitation. *Journal of the Atmospheric Sciences*, **61**, 1377–1391.

Tuleya R.E., DeMaria M. and Kuligowski R.J. (2007) Evaluation of GFDL and simple statistical model rainfall forecasts for U.S. landfalling tropical storms. *Weather and Forecasting*, **22**, 56–70.

Villarini G. and Smith J.A. (2009) Flood peak distributions for the eastern United States. *Water Resources Research*, submitted.

Willoughby H.E., Marks F.D. and Feinberg R.J. (1984) Stationary and moving convective bands in hurricanes. *Journal of the Atmospheric Sciences*, **41**, 3189–3211.

Q1 **Keywords:** •tropical cyclone; rainfall; quantitative precipitation forcasting; eyewall; rainbands; stratiform rain

QUERIES TO BE ANSWERED BY AUTHOR (SEE MARGINAL MARKS Q..)

IMPORTANT NOTE: You may answer these queries by email. If you prefer, you may print out the PDF, and mark your corrections and answers directly on the proof at the relevant place. Do NOT mark your corrections on this query sheet. Please see the proofing instructions for information about how to return your corrections and query answers.

Q1. As per style a minimum of 5 keywords are required. We have provided a few, please check.
Q2. Please confirm if the trim 'R−Z' should be changed to 'Z−R' in accordance with the text.
Q3. Please provide the part title for this article.
Q4. Please check and confirm if the copyright line provided in first page are ok.